2nd Mediterranean Conference on Fracture and Structural Integrity

Simulation of crack growth in residual stress fields of pre-fatigued T-welded joints repaired by tungsten inert gas: a 3D approach

Ramalho, A.L.[a,b]*, Antunes, F.[b], J.A.M. Ferreira[b]

aPolytechnic Institute of Castelo Branco, 6000-767 Castelo Branco, Portugal
bCEMMPRE, Department of Mechanical Engineering, University of Coimbra, 3004-516 Coimbra, Portugal

Abstract

In this article, a three-dimensional finite element model (FEM) is used to predict the crack growth at the weld toe of a pre-fatigued T-joint that was repaired with a remelting technique. The numerical models were developed using the MSC.Marc software. Fatigue life is estimated by integrating the Paris-Erdogan law. The stress intensity factors are obtained by the virtual crack closure technique (VCCT).

The T-welded joints, made of S355 steel, are obtained by covered electrode process and pre-cracked by fatigue. These welded joints were repaired by TIG dressing. The stress field generated by this dressing technique was estimated using a FEM model, presented in authors' previous works. For the crack growth was used the VCCT three-dimensional model recently presented by the authors to predict the effect of overloads. The pre-existence of an elliptical crack at the weld toe, with a depth of 0.5 mm was considered. It is also studied the growth of pre-existing cracks which have been poorly repaired.

It was observed that the TIG dressing produce residual compression stress fields on the weld toe that causes a delay in crack growth. The obtained results are compared with experimental ones. The fatigue's lives obtained by simulations with the numerical model presented in this paper allows to evaluate the application conditions of TIG remelting technique in the repair of pre-cracked welded joints.

Keywords: Type your keywords here, separated by semicolons ;

---

* Corresponding author. Tel.: +351 272 339 300; fax: +351 272 339 301.
  E-mail address: aramalho@ipcb.pt

1. Introduction

Currently, due to economic and environmental constrains, the use of the welded structures beyond their design lives is frequent, Manai (2021). In order for these structures to remain operational and within regulatory specifications, the defects detected in the monitoring programs need to be properly repaired.

In many structures the welds are the weakest link and as more high strength steels are developed and available on the market the demands for weld improvements increases, Jonsson *et. al* (2022). The benefits obtained by the TIG dressing improvement technique are attributed to the removal of flaws and the smoothing of the weld toe radius. The dressing techniques also modify the residual stress field at the weld toe section, Ramalho *et al.* (2011).

The use of these improvement treatments, as a repair techniques, has been reported by several authors, namely Branco *et al.* (2004), Ramalho *et al.* (2011), M. Edgren *et al.* (2019) and Al-Karawi *et al.* (2020).

The TIG remelting is one of the most efficient repair techniques of pre-cracked welded joints, Al-Karawi (2022). The efficiency of TIG remelting repair was evaluated using the simulation of crack growth at the weld toe, through numerical finite element models, Manai (2020).

In this work is presented a three-dimensional finite element model (FEM) used to predict the crack growth at the weld toe of a pre-fatigued T-joint that was repaired with TIG remelting technique. A previous 2D model, Ramalho *et al.* (2002), used to predict the residual stress field induced by TIG dressing, in T-welded joints, is upgraded to 3D. The fatigue life of pre-existing cracks at the weld toe is estimated by the integration of the Paris-Erdogan law. The stress intensity factor is obtained by the virtual crack closure technique (VCCT), implemented in the MSC.Marc software. The VCCT enable a local approach, considering the effect of the residual stress field on the stress intensity factor. A preliminary study is carried out, about the effect of the residual stress field generated by the TIG dressing, on the fatigue life of welded joints. The fatigue life prediction is compared with experimental values.

2. Introduction

2.1. Welding residual stress

A numerical model was built to simulate the TIG dressing process at the weld toe of an as-welded T-Joint. The 2D finite element model (FEM) used by Ramalho *et al.* (2002), was updated to 3D, including the investigations of Ramalho *et al.* (2018) about the material properties of the parent material, and the TIG welding efficiency proposed by Stenbacka *et al.* (2012) and Donegá *et al.* (2016).

The base material used in this study was a medium strength steel, S355, in the form of plates with 12.5 mm thickness. The welds were made by covered electrode process with weld metal in overmatching condition. T-joints weld specimens were produced from the main plates with low penetration fillet welded with an attachment of equal thickness. From this plate, specimens 70 mm wide and 270 mm long were cut. The weld leg length presented a medium value of 9 mm. Post-weld improvement and rehabilitation treatment of weld T-joints with fatigue cracks at the weld toe were performed by TIG dressing technique. Figure 1(a) shows the 3D geometry corresponding to half of a T welded joint specimen. The specimens were loaded in fatigue, by three-point bending.

The numerical simulation of the experimental work was performed in a virtual server running windows server 2016, Intel Xeon dual processor, with 128 RAM, using a FEM developed in the finite element software MSC.Marc 2018.The initial mesh consists of 19783 nodes and 98143 tetrahedral full integration linear elements. The element class was chosen according the posterior use of the model to simulate the generation and growth of cracks, in which the mesh was regenerated using the automatic algorithm Patran TetMesh, ensuring refinement in the weld toe and the symmetry of the geometry. The initial finite element mesh is represented in figure 1(b).

Thermal analysis

A 3D transient non-linear heat flow thermal analysis was carried out. The MSC.Marc, tetra 4, element type 135 was used. It's a four-node, isoparametric, solid linear element. This element uses linear interpolation functions and the thermal gradients are constant throughout the element. Adiabatic boundary conditions were considered in the

symmetry plane of the joint. In the base of the specimen was considered a heat sink as a fixed temperature boundary and in all the others surfaces, convective-radiative conditions were applied, Goldak *et al.* (1984).
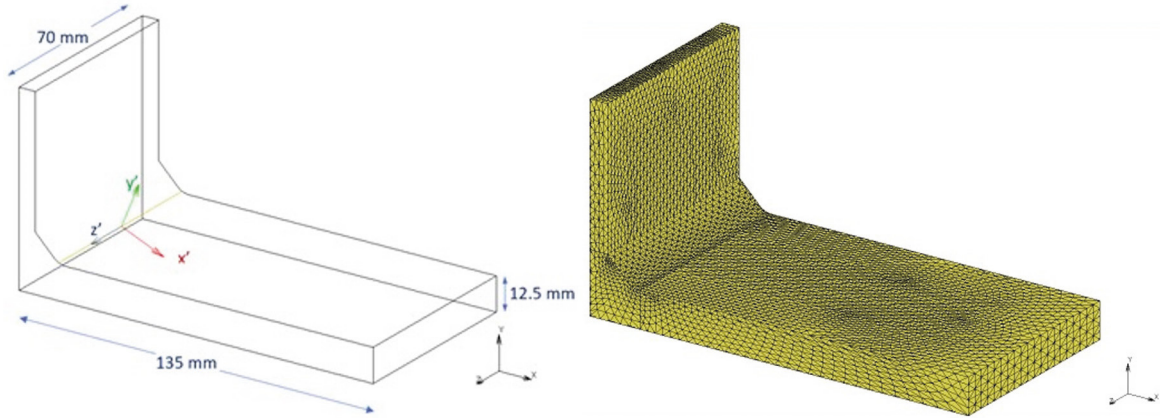

Fig. 1. (a) Geometrical model of the welded joint; (b) Initial mesh of the finite element model.

For the convective and radiative boundary conditions, a combined heat transfer coefficient was calculated using equation (1), Rykalin (1974).

$$h = 24.1 \times 10^{-4} \, \varepsilon \, T^{1.61} \tag{1}$$

where the T unit is °C, h unit is $Wm^{-2} \, °C^{-1}$ and ε is the emissivity of the surface of the body. From Ramalho *et al.* (2002) a value of 0.9 was assumed for ε.

The variation of the thermal conductivity with the temperature, K, was obtained from Ramalho *et al.* (2002). To take into account the influence of convection, caused by the fluid flow in the weld pool, the thermal conductivity was artificially increased for temperatures above the melting point. The variation of the specific heat with temperature, Cp, was obtained from Ramalho *et al.* (2018). A latent heat of fusion of 247 $kJkg^{-1}$ was assumed to be absorbed or released between the solidus and liquidus temperatures. These temperatures were assumed equal to 1470°C and 1520°C respectively, Ramalho *et al.* (2002). A constant density of 7860 kgm^{-3} was assumed for the steel.

The heat generated by the arc welding was inputted using the double ellipsoid heat source model, Goldak *et al.* (1984). In this model it is assumed a Gaussian distribution of the power density in the two half ellipsoids, with centre at point (0,0,0) and semi-axes a, b and c, parallel to the coordinate axes x', y', z', with origin at the beginning of the weld path as indicated in figure 1(a). With this model, the temperature gradient in the front of the heat source is steeper than the one that occurs at the rear half of the ellipsoid. The geometry of the double ellipsoid model is presented at figure 2, and their dimensions obtained from the macrography of the weld bead, from Ramalho *et al.* (2002).

The power density distribution in this model is done by equation (2).

$$q(x,y,z,t) = \frac{6\sqrt{3}f \, Q}{abc\pi\sqrt{\pi}} \, e^{-3x'^2/a^2} \, e^{-3y'^2/b^2} \, e^{-3z'^2/c^2} \, , \tag{2}$$

where Q is the heat input, Q=ηVI, η is the efficiency of the weld process, V is the voltage, and I the amperage. From Stenbacka (2012) and Donegá (2016) an efficiency of η=0.6 was assumed. From Ramalho *et al.* (2002) V= 110 V and I= 22 A. For the frontal semi-ellipsoid f=0.6, $c=c_1=3$ mm, a=2.4 mm and b=1.4 mm. For the rear semi-ellipsoid f=1.4 $c=c_2=6$ mm.
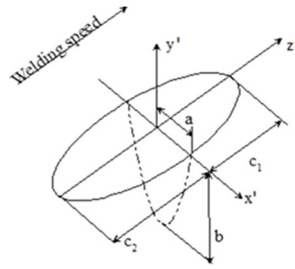
Fig. 2. Geometry of the double ellipsoid heat source model.

Structural analysis

A 3D quasi-static structural analysis was carried out with the same mesh that was used in the thermal analysis. The MSC.Marc Tetra 4 element type 134 was used. This is a four-node, isoparametric, solid linear element. This element uses linear interpolation functions and the strains are constant throughout the element.

In the symmetry plane, horizontal displacement restriction was performed. In the upper nodes on the right side, springs, with despicable stiffness, were added, in order to restrict the rigid body motion. The material was modelled as elasto-plastic, with a rate independent von Mises plasticity, using a combined hardening rule. The effect of microstructural changes on the generation of residual stresses was not considered, Börgesson and Lindgren (2001) and Barsoum and Barsoum (2009).The temperature-dependent mechanical properties were obtained from Ramalho *et al.* (2018).

The loading was performed by gradually imposing the deformation field originated by the temperature field obtained in the preceding thermal analysis, with a state variable boundary condition.

2.2. Fatigue crack propagation

Fatigue loading

From the experimental results presented in Ramalho *et al.* (2011), two paradigmatic cases were considered: the TR-D specimen where the TIG remelting promotes the integral repair of the pre-existing crack; and the TR-3 specimen, where the TIG remelting conducts to poor repair and from the pre-existing crack remains an embedded crack.

In the initial mesh is generated a semi-elliptical initial crack: for the TR-D specimen, with 0.5 mm of depth and a superficial length of 2 mm; for TR-3 specimen the crack is embedded being 3.3 mm deep and a length of 30 mm. This initial crack is generated in MSC Marc software by a faceted surface, through a remeshing process.

These models will be subjected to three-point bending fatigue, with a pulsating nominal load, corresponding to a stress range at the weld toe of 352.6 MPa for the TR-D specimen and 204.7 MPa for the TR-3 specimen, in two different initial conditions: with the initial stress field produced by the TIG remelting, previously estimated; without any initial stress field.

Crack propagation

The 2D crack propagation numerical model presented in Ramalho *et al.* (2020) used to evaluate the fatigue life of welded joints is here extended to 3D.

For the same T-welded joints analyzed in the present study, Ramalho *et al.* (2011), in a nominal approach, used the Mk factors proposed by Bowness and Lee (2000), to evaluate the stress intensity factor for the T-welded joint, under three-point bending with sinusoidal loading, with the equation (3).

$$K = M_k \sigma \sqrt{\pi a} \qquad (3)$$

The estimation of the fatigue life for the propagation period was carried out by integrating the Paris-Erdogan law, equation (4).

$$\int_{a_i}^{a_f} \frac{da}{\left(M_k \sqrt{\pi a}\right)^m} = \int_{N_i}^{N_f} C \Delta \sigma^m dN \qquad (4)$$

For the material propagation constants were used the values, $C = 1.2288 \times 10^{-8}$ and m= 2.6, with da/dN in mm/cycle and ΔK in MPa.m$^{1/2}$.

In present study, were maintained the three-point bending with sinusoidal loading and the material propagation constants. A local approach was used for the evaluation of the stress intensity factor, through the evaluation of the strain energy release rate (G). This model is valid in the elastic domain. The propagation of a crack occurs when the energy released equals the fracture toughness of the material. In the VCCT is assumed that, for an infinitesimal crack opening, the strain energy released equals the amount of the work required to close the crack. To simplify the evaluation of this work, is assumed that an infinitesimal crack extension, Δa, has negligible effects on the crack front, therefore the stress and displacement fields can be evaluated at the same configuration, Krueger (2004) and Elisa (2011). In the mode I of fracture, opening mode, G is evaluated by equation (5).

$$G_I = \lim_{\Delta a \to 0} \frac{1}{2\Delta a} \left(\int_0^{\Delta a} \sigma_{yy}^{(a)} \delta u_y^{(a)}(x - \Delta a)dx + \int_0^{\Delta a} \sigma_{yx}^{(a)} \delta u_x^{(a)}(x - \Delta a)dx \right.$$
$$\left. + \int_0^{\Delta a} \sigma_{yz}^{(a)} \delta u_y^{(a)}(x - \Delta a)dx \right), \qquad (5)$$

where the superscript (a) means that displacements and stress are evaluated in the model with the crack length a.

For 3-D solids, the G evaluation is done separately at each node on the crack front and the area of influence of these nodes is half of the areas of the contiguous elements. Each node at the crack front is considered as an individual crack.

Equation (5) can be adapted to the mode II and III of fracture. For plane strain and 3D analysis the stress intensity factors can be found by equations (6).

$$G_I = (1 - v^2)\frac{K_I^2}{E}, \quad G_{II} = (1 - v^2)\frac{K_{II}^2}{E}, \quad G_{III} = (1 + v)\frac{K_{III}^2}{E} \qquad (6)$$

Equations (5) and (6) permit the evaluation of stress intensity factors, in the presence of stress residual fields.

The initial crack is generated by automatic remeshing using a faceted surface. This initial crack is propagated by fatigue. In fatigue crack propagation, a load sequence is repeated a number of times. After each sequence, cracks are grown. For high cycle fatigue, a maximum growth increment was specified, which is scaled along crack fronts. This scaling allows the determination of the shape of the crack front during growth. a maximum crack growth increment of $\Delta a0 = 0.25$ mm was considered, and a scaling of this increment to each node on the crack front (Δa) based on equation (7), Marc (2018).

$$\Delta a = \frac{\Delta a^{fat}}{\Delta a_{max}^{fat}} \Delta a_0 \qquad (7)$$

where Δa^{fat} is the growth increment for each crack-node in the crack front, calculated by the Paris-Erdogan law using the respective ΔK. To ensure that the crack fronts stay smooth, were used a smoothing scheme based upon running averages for the growth increments along the front.

In this approach the crack length increment, Δa_0, was prescribed and the corresponding number of fatigue cycles, N, was calculated by the integration of Paris-Erdogan Law (4), assuming a linear variation of the stress intensity factors K along the increment of the crack.

3. Results and discussion

3.1. Fatigue crack propagation

In figures 3(a) and 3(b) are presented the von Mises stress and the longitudinal plastic strain fields (ε_{pxx}), generated by TIG dressing, respectively. There is a well-defined peak of stresses and strains at the root of weld toe, induced by the thermal process. The maximum values of stresses are above 500 MPa. Along the width of the specimen, there is no significant variation in the stresses. The field of stresses and deformation are similar and in good agreement with the results presented by other authors, Barsoum and Barsoum (2009) and Yuan and Sumi (2013).

The estimated residual stresses, σ_{xx}, near the weld toe were compared with the ones obtained by Ramalho *et al.* (2020). Figure 4 presents the variation of σ_{xx} residual stresses versus the distance x. The increase of x distance produces an increase of residual stresses up to a peak, followed by a progressive decrease. A good agreement is observed between the numerical predictions and experimental values obtained by X-ray diffraction and hole drilling technique, which validates the numerical procedure. x_{toe} corresponds to the position of the weld toe, measured from the symmetry plane, being used to allow comparison between different specimens.
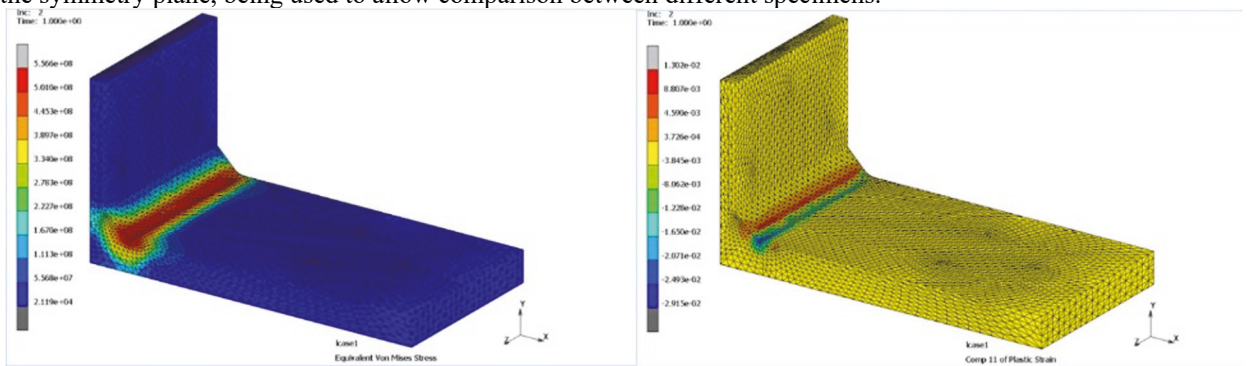

Fig. 3. (a) Estimated von Mises residual stress field [Pa]; (b) Estimated longitudinal plastic strain fields.
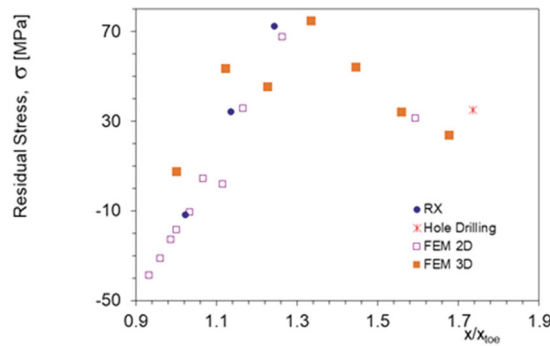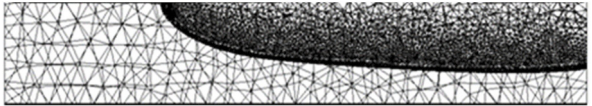

Fig. 4. Comparison between the estimated residual stresses and those obtained experimentally.

3.2. Crack propagation lives

In table 1 are presented the estimated lives for the TR-D specimen, where the TIG remelting conduces to the integral repair of pre-existing fatigue cracks with depths a_r lesser than 2.5 mm. The nominal stress range at the weld toe is represented by $\Delta\sigma$, and $N_{estimated}$ and $N'_{estimated}$ correspond respectively to the lives obtained by the numerical simulations with and without the initial residual stress field generated by TIG dressing. $N_{exper.}$, corresponds to the experimental life published in Ramalho *et al*. (2011).

Table 1. Experimental and predicted values of fatigue lives for the TR-D specimen.

a_r [mm]	$\Delta\sigma$ [MPa]	$N_{exper.}$	$N_{estimated}$	$N'_{estimated}$	Estimated fracture surface
<2.5	352.6	628739	572837	531627	

The numerical model produces very good estimations for the life after reparation of TR-D specimen. The estimated lives with and without initial stress fields present a deviation from the experimental one of 9% and 15%, respectively. In figure 5 is shown the fracture surface that occurs in the TR-D specimen.
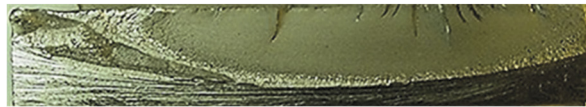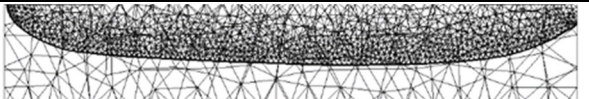

Fig. 5. Fracture surface of TR-D specimen.

The estimated geometry for the final configuration of the crack is close to what occurs in the TR-D specimen.
In table 2 are presented the estimated lives for the TR-3 specimen, where the TIG remelting conduces to the poor repair of pre-existing fatigue crack with the depth a_r equal to 4.8 mm.

Table 2. Experimental and predicted values of fatigue lives for the TR-3 specimen.

a_r [mm]	$\Delta\sigma$ [MPa]	$N_{exper.}$	$N_{estimated}$	$N'_{estimated}$	Fracture surface
4.80	204.7	361890	391110	322299	

The numerical model produces very good estimations for the life after reparation of TR-3 specimen. The estimated lives with and without initial stress fields both present a deviation from the experimental one of 11%, the first by excess and the second by default. In figure 6 is shown the fracture surface that occurs in the TR-3 specimen, where is visible that the TIG remelting produces an approximately semi elliptic embedded crack with the dept h of 3 3 mm and the length of 30 mm.

Fig. 6. Fracture surface of TR-3 specimen.

The estimated geometry for the final configuration of the crack is close to what occurs in the TR-3 specimen. From the lives estimated for both the simulations we drawn that the compression stress field generated by TIG remelting causes a delay in crack growth.

The preliminary results obtained for the presented 3D numerical model are consistent with those obtained experimentally, and produces much more accurate estimates than those obtained in the previous 2D model presented in Ramalho *et al.* (2020).

4. Conclusions

A two-step thermo-mechanical finite element analysis was applied to predict residual stress field, induced by TIG dressing at the weld toe of a T-joint, using a 3D transient non-linear thermal analysis followed by a 3D structural quasi-static elasto-plastic one.

Predicted and experimental surface residual stresses obtained by the X-ray diffraction method, were compared and a very good agreement was obtained.

A 3D numerical model for estimating fatigue life using the VCCT was developed and presented. This model reveals to be effective to predict the growth of cracks at the weld toe of a T joint. This model evaluates the influence of residual stresses generated by the TIG remelting process at the weld toe, on the crack propagation speed. The model was successfully applied in estimating the growth of embedded cracks resulting from poor repairs.

Acknowledgements

References

Al-Karawi, H., 2022. Literature review on crack retrofitting in steel by Tungsten Inert Gas remelting. Ships and Offshore Structures, DOI: 10.1080/17445302.2021.2020986.

Al-Karawi, H., Polach, R.U.F.B., Al-Emrani, M., 2020. Fatigue crack repair in welded structures via tungsten inert gas remelting and high frequency mechanical impact. Journal of Constructional Steel Research 172: 106200.

Barsoum, Z., Barsoum, I., 2009. Residual stress effects on fatigue life of welded structures using LEFM. Engineering Failure Analysis, 16:1, 449-467.

Börgesson, L., Lindgren, L-E., 2001. Simulation of Multipass Welding With Simultaneous Computation of Material Properties. Journal of Engineering Materials and Technology, 123:1, 106-111.

Bowness, D., Lee, M.M.K., 2000. Prediction of weld toe magnification factors for semi-elliptical cracks in T butt joints. International Journal of Fatigue, 22:5, 369-387.

Branco, C.M., Infante, V. Baptista, R., 2004. Fatigue behaviour of welded joints with cracks, repaired by hammer peening. Fatigue Fract Eng Mater Struct 27(9):785–98.

Donegá T.J., Costa, T. F., Rosenda, V. A., Vilarinho, L. O., 2016. Comparison of thermal efficiency between A-TIG and conventional TIG welding. Welding International, 30:4, 255-267.

Edgren, M., Barsoum, Z., Åkerlind, K., Al-Emrani, M., 2019. Evaluation of HFMI as a Life Extension Technique for Welded Bridge Details. Procedia Structural Integrity 19: 73–80.

Elisa, P., 2011. Virtual Crack Closure Technique and Finite Element Method for Predicting the Delamination Growth Initiation in "Composite Structures Advances in Composite Materials: Analysis of Natural and Man-Made Materials". In: Tesinova, P. (Ed.). In Tech, Rijeca, Croatia, pp. 463.

Goldak, J., Chakravarti, A., Bibby, M., 1984. A New Finite Element Model for Welding Heat Sources. Metallurgical Transactions B, 15B, 299-305.

Jonsson, T., Narström, T., Barsoum, Z., 2022. Fatigue and Ultimate Strength Assessment of Post Weld Treated. Procedia Structural Integrity 38, 411-417.

Krueger, R., 2004. Virtual crack closure technique: History, approach and applications. Applied Mechanics Reviews, Vol. 57:2, 109-143.

Manai, A., 2020. A framework to assess and repair pre-fatigued welded steel structures by TIG dressing. Engineering Failure Analysis 118: 104923.

Manai, A., 2021. An analysis of pre-fatigued TIG-treated welded structures. Engineering Failure Analysis (2021) 121: 105150.

Marc 2018. Volume A: Theory and User Information. User Documentation, MSC Software Corporation.

Ramalho, A.L., Antunes, F., Ferreira, J.A.M., 2020. Crack Growth In Simulated Residual Stress Fields On Tungsten Inert Gas Dressed Welded Joints – A 2D Approach. Anales de la Mecânica de la Fractura, 104-109.

Ramalho, A.L., Antunes, F., Nobre, T., Ferreira, J.A.M., 2018. Caraterização Mecânica do Aço S 355 a Temperatura Elevada, TEMM2018 – 1st Iberic Conference on Theoretical and Experimental Mechanics and Materials, 4-7 November, Porto, Portugal.

Ramalho, A.L., Ferreira, J.A.M., Branco, C.M., 2002. Residual stresses analysis in TIG dressed welded joints, The 8th Portuguese Conference on Fracture, 20-22 February, Vila Real, Portugal.

Ramalho, A.L., Ferreira, J.A.M., Branco, C.M., 2011. Fatigue Behaviour of T Welded Joints Rehabilitated by Tungsten Inert Gas and Plasma Dressing. Materials and Design, 32:10, 4705-4713.

Rykalin, R.R., 1974. Energy Sources for Welding. Houdrement Lecture, International Institute of Welding, London.

Stenbacka, N., Choquet, I., Hurtig, K., 2012. Review of Arc Efficiency Values for Gas Tungsten Arc Welding, IIW Commission IV-XII-SG212 Intermediate Meeting BAM. Berlin, Germany 18-20 April, Doc. XII-2070-12/212-1229-12.

Yuan, K., Sumi, Y., 2013. Welding residual stress and its effect on fatigue crack propagation after overloading in "Analysis and Design of Marine Structures". In: – Guedes Soares & Romanoff, J., Soares, C. G. (eds). Taylor & Francis Group, London, pp. 447.